Experimental Verification of Backscattering Protection in PTD-Symmetric Bifilar Edge Waveguides

Iram Nadeem, *Student Member, IEEE*, Valentina Verri, Enrica Martini, *Senior Member, IEEE*, Fabio Morgia, Alberto Toccafondi, *Senior Member, IEEE*, Maurizio Mattivi, and Stefano Maci, *Fellow, IEEE*

***Abstract*— This article presents the design and experimental characterization of microwave structures based on parity time-reversal duality symmetric bifilar edge waveguides (PTD-BEWs) realized through a parallel plate waveguide (PPW) loaded by a metasurface. The analyzed structures include transmission lines with bends and multiple line arrangements. Due to their unique symmetry properties, these structures are robust against backscattering, thus resembling the behavior of topological WGs, despite the fact they are reciprocal. This makes it possible to guide the electromagnetic (EM) waves along the edge with low insertion losses and unique matching properties. Measurements, performed in the frequency range between 24 and 32 GHz, have confirmed the feasibility of the theoretical concept.**

***Index Terms*— Boundary conditions (BCs), edge waveguide (WG), parity time-reversal duality (PTD) symmetry, substrate integrated WG (SIW), topological modes.**

I. Introduction

In THE recent years, topological edge modes have drawn considerable attention due to their unidirectional property, which implies inherent immunity to backscattering at discontinuities [1]. These edge modes are normally supported at the interface of two nonreciprocal media with different Chern numbers [2]–[6]. However, recent research studies have shown that a similar robust propagation can also be achieved in reciprocal structures exhibiting parity time-reversal duality (PTD) symmetry. The topological insulators introduced in [7] are particular examples of reciprocal systems with an Ω-type bianisotropic coupling. In general, a waveguiding structure is named PTD-symmetric if it is invariant under the combination of parity, time-reversal, and duality transformations. It was first shown in [8] that bidirectional PTD-symmetric N-port networks are characterized by a scattering matrix with vanishing diagonal elements, that is, $S_{11} = \cdots\cdots = S_{NN} = 0$. Thus, a PTD-invariant microwave network is always matched at all ports. Quite remarkably, this property can also be achieved in passive, lossless, and reciprocal guiding structures, which implies a significant simplification for practical realization with respect to active or nonreciprocal solutions. In fact, since passive, lossless, and reciprocal structures are time-reversal symmetric, PTD symmetry, in this case, is achieved anytime an axis exists in the transverse cross section whose inversion produces dual boundary conditions (BCs) with respect to the original ones [see Fig. 1(a)]. Propagation in such guiding structures will be unaffected by any perturbation or defects that do not break the PTD symmetry. It is noted that also the perturbation introduced by termination into free space belongs to this class. Different symmetry-protected waveguides (WGs) proposed in the literature can be cast in this framework [9]–[11]. In particular, the WG introduced in [10] consists of a junction between two planar surfaces characterized by complementary impedance BCs (capacitive and inductive). This structure supports an edge mode, whose field is tightly confined in the proximity of the junction; such a mode exhibits highly efficient propagation also along nonrectilinear paths, as experimentally demonstrated in [12]. However, the structures in [10] and [12] are open; as a consequence, their Green's functions are characterized by a continuous spectrum of modes, and therefore, even if there is no backscattering at PTD-symmetric discontinuities, there can be radiation losses. In contrast, a PTD-symmetric WG with a closed cross section does not suffer from this impairment. Examples of this latter class of guiding structures are presented in Fig. 1. In particular, the square cross section structure in Fig. 1(b) has been studied in [9]. An array of such open-ended WGs has been investigated in [13] and [14]. The array elements are arranged so that the overall structure still satisfies PTD-symmetry with respect to multiple axes, and this allows one to obtain wide-angle beam scanning with good matching performance.

An alternative structure, represented in Fig. 1(c), was proposed and analyzed in [11]. It is obtained by pairing two semi-infinite parallel plate WGs (PPWs) with swapped perfect electric conducting (PEC) and perfect magnetic conducting (PMC) BCs. This structure satisfies PTD-symmetry with respect to the direction normal to the two plates [11], [15] and, for separation between walls less than a quarter of a wavelength, it supports a unique mode strongly confined at the edges between PEC and PMC. For this reason, we denote this guiding structure as a bifilar edge waveguide (BEW).

Manuscript received 30 December 2021; revised 20 May 2022; accepted 19 June 2022. Date of publication 21 July 2022; date of current version 17 November 2022. *(Corresponding author: Stefano Maci.)*

Iram Nadeem, Enrica Martini, Alberto Toccafondi, and Stefano Maci are with the Department of Information Engineering and Mathematics, University of Siena, 53100 Siena (SI), Italy (e-mail: macis@ing.unisi.it).

Valentina Verri, Fabio Morgia, and Maurizio Mattivi are with the Milan Research Center, Huawei Technologies, 20147 Milan (MI), Italy.

Color versions of one or more figures in this article are available at https://doi.org/10.1109/TAP.2022.3191422.

Digital Object Identifier 10.1109/TAP.2022.3191422

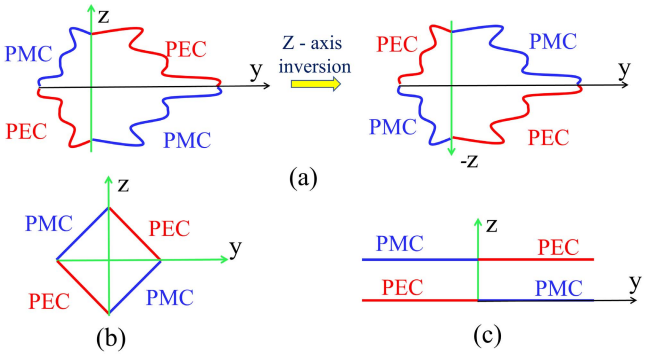

Fig. 1. Examples of cross sections of PTD-symmetric WGs. (a) PTD-symmetric WG where the z-axis is the parity axis. (b) Square cross section structure with two parity axes (both z- and y-axes). (c) BEW-PPW WG with z-axis as parity axis, which is a simplified model for the structure discussed in this article.

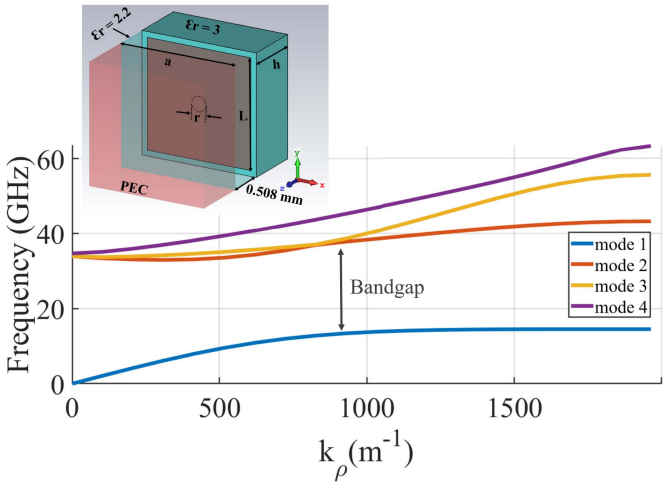

Fig. 2. Dispersion diagram of the PEC-covered mushroom metasurface.

This PTD-BEW is numerically and experimentally investigated in this article. In particular, we present here experimental evidence of robust unidirectional propagation in PTD-BEW, implementing the geometry at Ka-band by means of mushroom metasurfaces [16] to realize the PMC. In the simulations, rectangular WGs (RWGs) have been used to excite the structure. In the realization, the RWG is substituted by a grounded co-planar WG (GCPW) to benefit from the printed circuit board (PCB) technology.

This article is organized as follows: Section II presents the design of the PTD-BEW unit cell based on the mushroom surface. Section III introduces different structures based on the PTD-BEW and shows the relevant simulated results. Section IV gives details about the prototype assembling technology and the realized feeding structure. Section V provides the measured results for the manufactured PTD-BEW structures. Finally, Section VI draws the concluding remarks.

II. Dispersion of PTD-BEW

The practical implementation of the WG in Fig. 1(c) is performed by using a mushroom-type metasurface to emulate PMC BC. The unit cell of this metasurface consists of a square patch printed on a grounded dielectric substrate and connected to the ground plane through a central via, as shown in the inset of Fig. 2. In the ideal case of Fig. 1(c), each half of the structure consists of a PPW with PEC/PMC BCs on the two plates; for separation distances between walls smaller than a quarter of a wavelength, such a WG does not support any modal propagation. In the practical implementation, the PMC is substituted by a mushroom metasurface designed to exhibit high impedance in the desired frequency band. This way, each half of the PTD-BEW, which consists of the mushroom metasurface covered by a metal plate, individually exhibits a bandgap in the same frequency band. A parametric study has been carried out in order to optimize the mushroom unit cell. Finally, the following geometrical parameters have been selected: size of the unit cell $a = 1.6$ mm, side of the square patch $L = 1.45$ mm, and via radius $r = 0.1$ mm. The space between the PEC wall and the top of the mushroom is filled by a dielectric with relative permittivity $\epsilon_r = 2.33$ and has a thickness $d = 0.508$ mm. The resulting structure has been analyzed with Simulia CST. The dispersion diagram, reported in Fig. 2, exhibits a bandgap between 15 and 32 GHz.

When the WG in Fig. 2 is paired with an analogous structure with PEC on the bottom and mushroom on top, the two edge-lines at the junction support a bifilar edge wave, whose field is exponentially attenuated on the two sides $x > 0$ and $x < 0$ with a penetration depth (inverse of the attenuation constant) approximately equal to the separation distance between the top surface of the mushroom and the PEC wall d. Since the field is confined between the two edge lines, the structure resembles a bifilar transmission line. The dispersion diagram of this structure is reported in Fig. 3 along with the light line in the filling dielectric. It is worth noting that the light line crosses the BEW dispersion curve at the frequency where the mushroom surface better emulates the PMC. Around this point, the edge mode is quasi-transverse EM (TEM). In fact, for the ideal PEC-PMC BCs, the supported mode is TEM [11], [15], but the practical implementation of the PMC through mushrooms introduces a limited dispersion, so that the mode will be quasi-TEM. It is noted that around the central frequency, at which the mode is quasi-TEM, the dispersion curve crosses the light line, which means that around that frequency the mode exhibits a transition from a fast wave to a slow wave. This occurs also in other closed guiding structures with impedance-loaded walls, for example, in the realization of the WG in Fig. 1(b) with practical high impedance surfaces, due to the fact that the impedance of the walls changes from inductive to capacitive [17]. As opposed to the case of ideal PEC/PMC BCs, this transition is associated with a group velocity smaller than the speed of light. Despite this effect, the backscattering protection seems to be preserved.

The unimodal bandwidth ranges from 19.36 GHz (the cut-off frequency of the edge mode) to 32.57 GHz (the cut-off frequency of the higher order mode), corresponding to a percent bandwidth of approximately 50%. However, the percentage bandwidth in which the structure is expected to approach the ideal behavior, represented by the shaded area in Fig. 3), is around 20%.

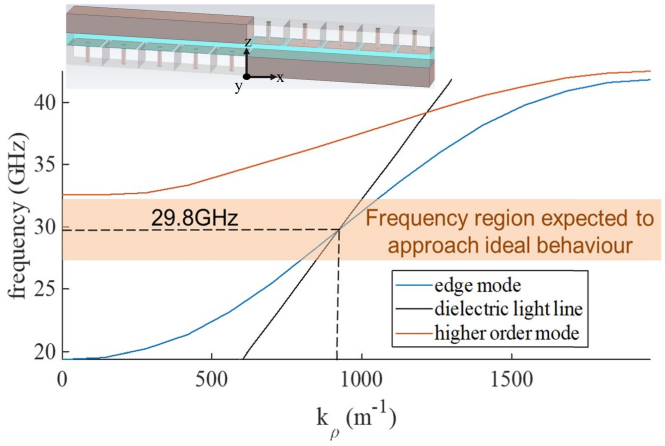

Fig. 3. Dispersion diagram of the PTD-BEW. The black line represents the light line in the dielectric filling the WG.

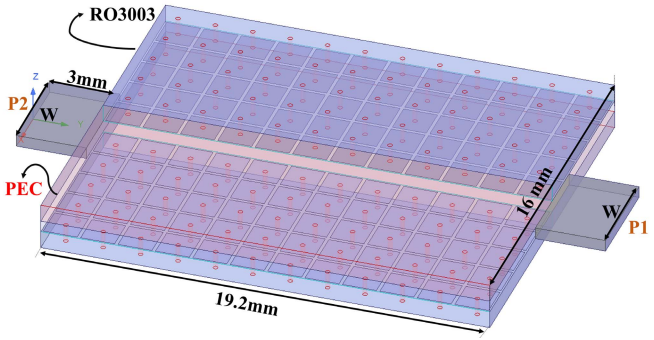

Fig. 4. Branch of BEW fed by RWGs.

III. PTD-Symmetric Basic BEW Structures

The first considered structure, represented in Fig. 4, has been used to design a practical feeding arrangement to excite the PTD-BEW. It consists of a branch of PTD-BEW based on the basic unit cell introduced in Section II and shown in Fig. 3, connected at the two sides to two sections of RWG. The height of the RWG has been set equal to the distance between the mushroom surface and PEC wall in the PTD-BEW (i.e., 0.508 mm), and its width has been varied to obtain a good matching over the frequency band of interest. A parametric study has been conducted on HFSS to this end. The reflection coefficients resulting from this parametric study, with the width W ranging between 4.1 and 4.8 mm, are reported in Fig. 5. For the smallest size, the low-frequency peak corresponds to the cut-off frequency of the WG; results are therefore to be considered significant only above that frequency. Fig. 6 presents the amplitude of the transmission coefficient for different values of W. The best matching performance in the frequency range between 25 and 32 GHz is obtained for $W = 4.3$ mm. This value makes the modal impedance of the TE_{10} mode of the RWG close to the intrinsic impedance of the TEM-BEW.

Fig. 7 presents a snapshot of the amplitude of the electric field inside the WG. As can be seen, the field is confined at the bifilar junction of PEC and mushroom, with a penetration distance approximately equal to a couple of mushroom unit cells. Leakage away from the junction is prevented by the bandgap of the PPW with dual BCs, which extends up to 32 GHz. A certain coupling of the RWG with the lateral edges in the front is also perceivable from the picture.

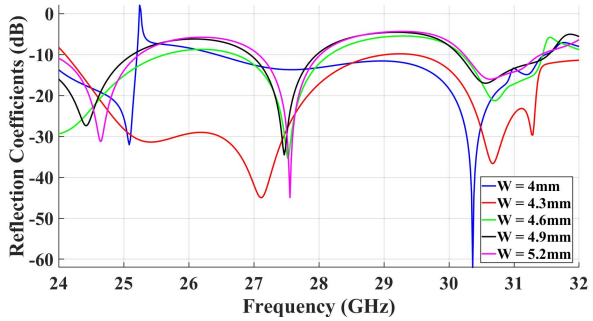

Fig. 5. Simulated reflection coefficient for different values of the RWG width W.

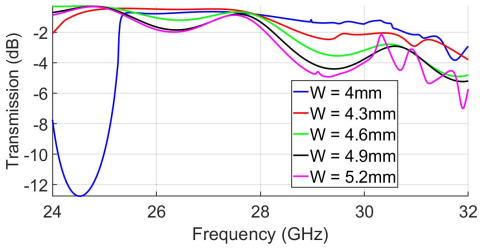

Fig. 6. Simulated transmission coefficient for different values of the RWG width W.

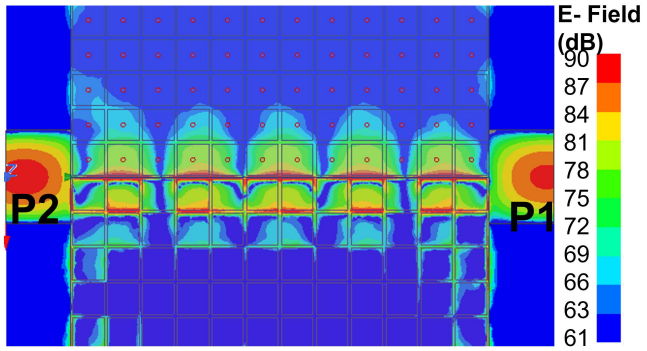

Fig. 7. Snapshot of the electric field in the central longitudinal section of the structure in Fig. 4 when the port on the left (P2) is excited.

Once the feeding structure has been designed, other configurations can be analyzed. Fig. 8 shows a WG path with 90° bends (segmented PTD-BEW). This structure serves to test the robustness of the guiding structure against reflections. The PTD-BEW is entirely enclosed by metallic walls laterally. From the simulated S-parameters reported in Fig. 9, we observe that reflection at the input port is limited over the entire bandwidth. The reflection coefficient is below −20 dB in the frequency range between 29.5 and 31.5 GHz, where the PTD-BEW is expected to better emulate the ideal behavior (see Fig. 3). It is worth noting that these results also include the effect of the two transitions to RWG, which are the major cause of reflections. A snapshot of the electric field in the

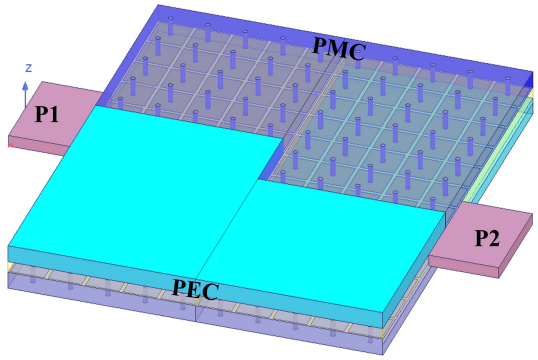

Fig. 8. PTD-BEW path with 90° bends. The light blue color denotes the PEC part of the top wall.

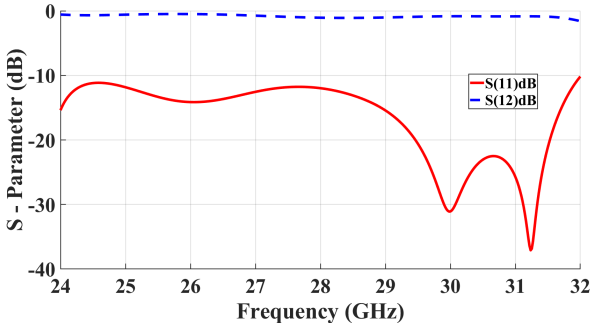

Fig. 9. Simulated reflection coefficient of the BEW with 90° bends.

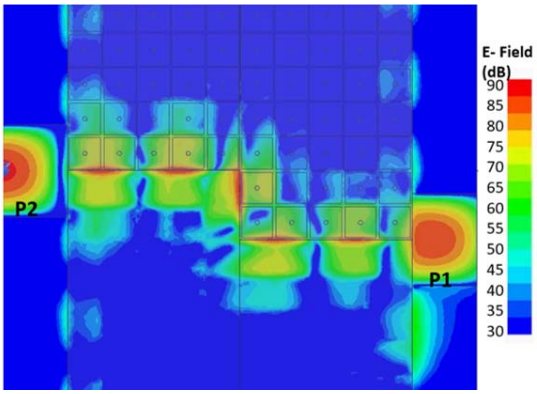

Fig. 10. Snapshot of the electric field in a longitudinal cross section for the PTD-BEW with 90° bends.

longitudinal cross section can be seen in Fig. 10. We observe that the field is properly confined at the edge throughout the entire path and the propagation follows the bends.

IV. Detailed Prototype Design

PTD-BEW prototypes have been realized in PCB technology. The stratification of the prototypes is shown in Fig. 11. Three layers of dielectric materials are glued together by means of two layers of Astra MT77 Prepreg 1035LD of the thickness of 0.126 mm each. The first dielectric layer is Rogers RO3003 of thickness 0.762 mm, with a top metalization made by copper of 0.06 mm and a bottom one of 0.05 mm. The third layer is also of the same material as the first one, with 0.05 mm

Fig. 11. Stack-up of the prototypes.

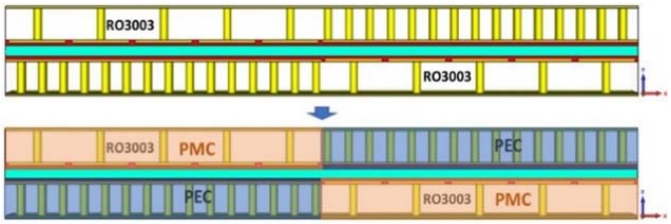

Fig. 12. Transverse cross section of the PTD-BEW. The prepreg is represented in red, copper in yellow, and Rogers RT5870 in light blue. The bottom picture highlights the regions emulating the ideal PEC/PMC BC.

metalization on the top and 0.06 mm on the bottom. In between those two layers of RO3003 (used for the realization of the mushroom metasurface), there is a layer of Rogers RT5870, which has $\epsilon_r = 2.33$ and electric loss tangent equal to 0.0012. Fig. 12 shows the cross section of the PTD-BEW structure transverse to the propagation direction. The region that should act as PEC is created by a dense distribution of metallic vias made of copper crossing the RO3003 layer, while the mushroom surface is realized in the same dielectric layer, with the external metalizations acting as ground planes and the patches created in the inner metalizations and connected to the external copper layer by vias. All vias have a radius of 0.2 mm and the mushroom patches are immersed in the prepreg.

The examples discussed in Section III are with RWG feeding. An alternative solution more convenient for PCB realization, and including transitions to SMA connectors is presented in Fig. 13. This solution includes a transition from a G-CPW to a substrate-integrated WG (SIW), which is used to feed the PTD-BEW [18]–[20]. The basic rules for the design of the SIW are provided in [21] and [22].

The central strip of the G-CPW has an initial width of $w_0 = 1.56$ mm to exhibit 50 Ω at the input port, while the width at the end of the tapered section is $W = 4.3$ mm. The lengths $L1$ and $L2$ of the tapered and nontapered sections are approximately 12 mm. The diameter of the vias for the feeding structure is $d = 0.5$ mm. There are few metallic vias of 0.7 mm crossing all the dielectric layers (both RO3003 and RT5870) enclosing the PTD-BEW to support the handling of the structure.

The strip of the G-CPW is printed at the same level as the mushroom surface patches. Taking into account the additional thickness due to the presence of the prepreg, the thickness of the RT5870 was taken to equal to 0.254 mm in order to achieve performance similar to the ones obtained without prepreg and a thickness of 0.508 mm. The branch of PTD-BEW includes 12 unit cells, and the total length of the structure, including the feeding sections, is 43.8 mm. A length corresponding to five unit cells of the mushroom metasurface has been considered in the transverse direction for each side; the overall width of

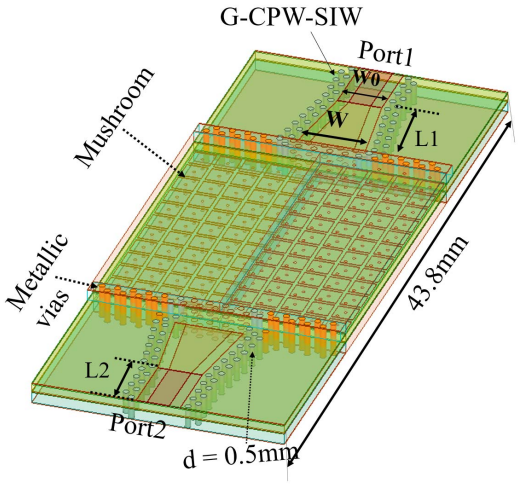

Fig. 13. Straight PTD-BEW section fed by a G-CPW port. The feeding structure includes a transition to SIW.

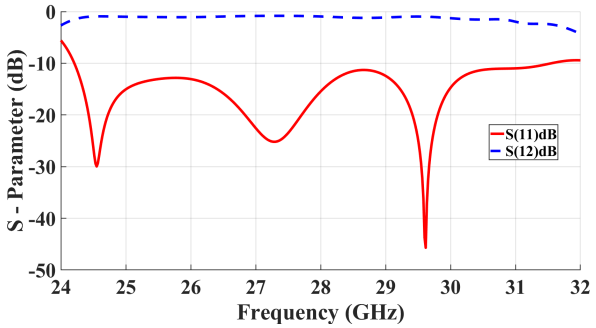

Fig. 14. Simulated scattering coefficients of the structure shown in Fig. 13.

the structure is 16.5 mm. The simulated scattering coefficients of this structure are shown in Fig. 14. The structure exhibits good matching over the whole bandwidth from 25 to 32 GHz and low losses (the transmission coefficients are larger than −1 dB up to 30.5 GHz, with an average value of 0.6 dB).

The second considered structure is an arrangement of parallel PTD-BEWs and it is used to investigate the mutual coupling between them. Five pieces of BEW WGs are realized in the same PCB to obtain a multiple port configuration as shown in Fig. 15. Each BEW has four mushroom unit cells for each side in the transverse cross section, and the same four unit cells are shared by two adjacent WGs. It is important to note that there is no physical separation between the various BEW structures. The distance between the centers of adjacent line ports (and therefore between adjacent edge junctions) is 8 mm which is approximately 0.8 free space wavelengths. The simulated scattering coefficients are reported in Fig. 16. It can be seen that the coupling is always lower than −30 dB between ports located on the same side, and below −20 dB for ports located on opposite sides. At the same time, the matching of each channel appears unaffected by the presence of the other channels.

V. Measurements

A. Straight PTD-BEW Section

Fig. 17 shows a picture of the realized prototype of a straight PTD-BEW section fed with a GCPW-to-SIW

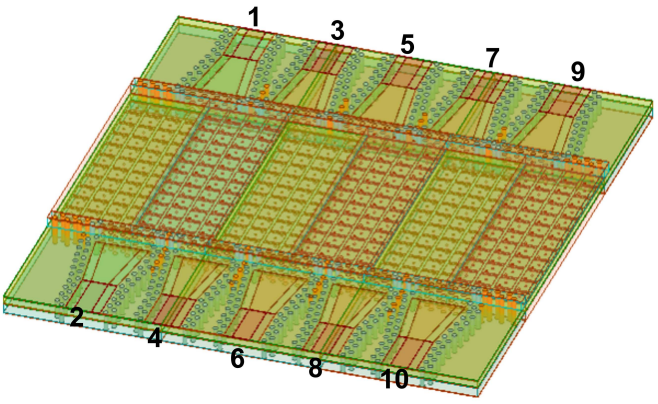

Fig. 15. Multiport PTD-BEW structure in which five BEW sections are arranged together.

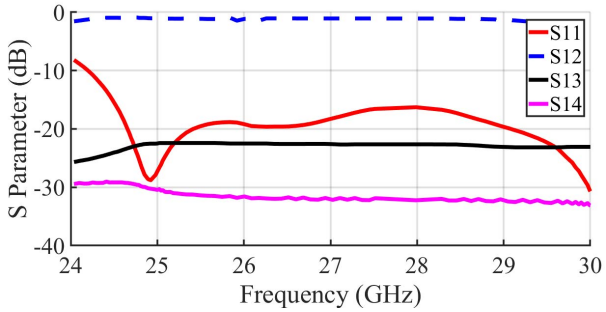

Fig. 16. Simulated coupling coefficients for the structure in Fig. 15.

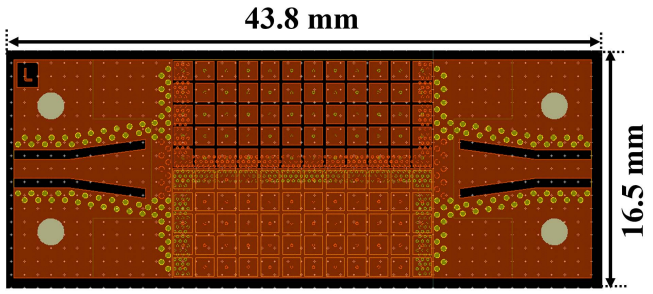

Fig. 17. Layout of the realized PTD-BEW section with GCPW-to-SIW transitions.

transition, according to the design presented in Section IV. Fig. 18 shows the measured scattering parameters in a range from 20 to 36 GHz. It is seen that the structure presents a reflection coefficient smaller than −7.5 dB across the whole band from 24 to 31 GHz, and smaller than −15 dB within the subband from 24 to 26.5 GHz. The transmission coefficient is around −1.5 dB between 24 and 31.5 GHz. The discrepancy with respect to simulations is thought to be due to realization imperfections and higher losses in the real materials. Fig. 19 shows a different realization of a straight PTD-BEW section with GCPW-to-SIW transition. In this case, only three mushroom unit cells are used in the transverse direction, while 12 unit cells are used in the longitudinal direction. The measured results for this structure are illustrated in Fig. 20; the reflection coefficient is generally lower than in the previous

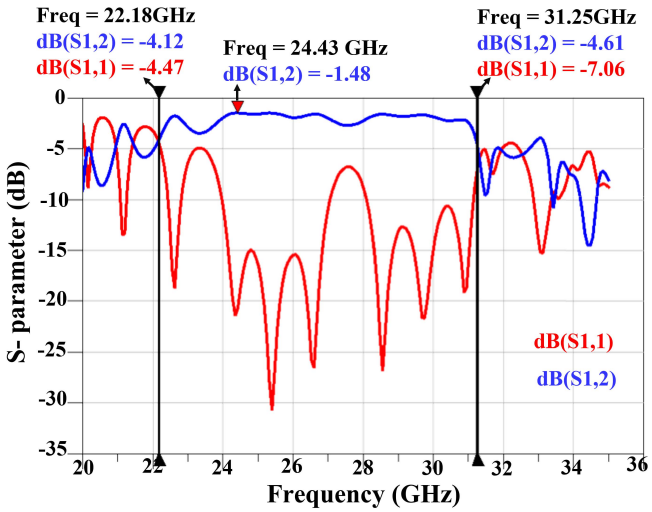

Fig. 18. Measurements of S_{12} (blue line) and S_{11} (red line) in the range 20–36 GHz.

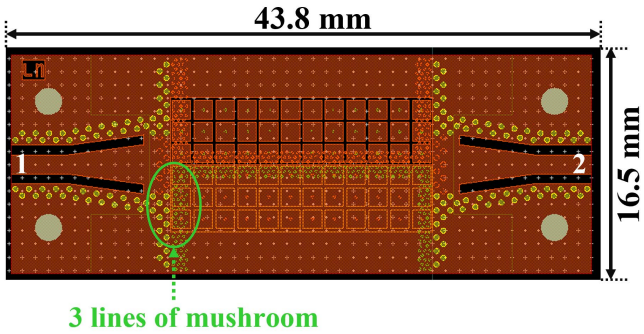

Fig. 19. Layout of the PTD-BEW section with GCPW-to-SIW transitions with a smaller number of mushroom unit cells.

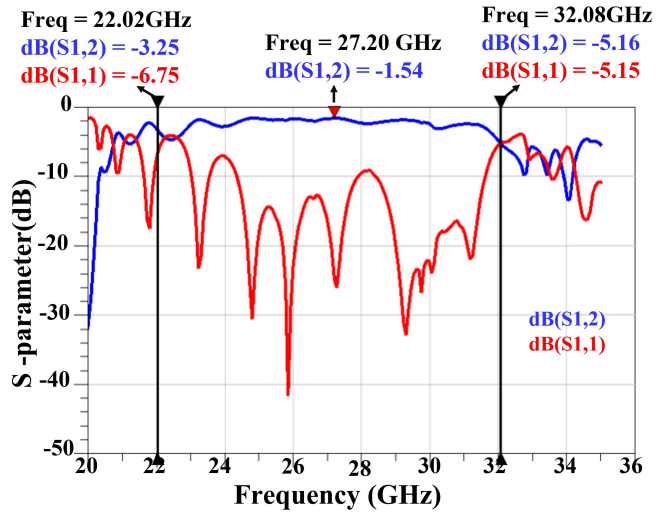

Fig. 20. Measurements of S_{12} (blue line) and S_{11} (red line) in the range 20–36 GHz for the layout shown in Fig. 19.

case, with bandwidth at −9.5 dB between 24.5 and 31.5 GHz, probably due to a better realization. The insertion loss is still around −1.5 dB.

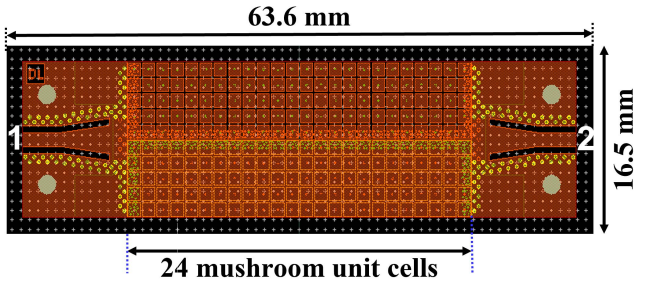

Fig. 21. Layout of a PTD-BEW section with 24 mushroom unit cells in the longitudinal direction and GCPW-to-SIW transitions.

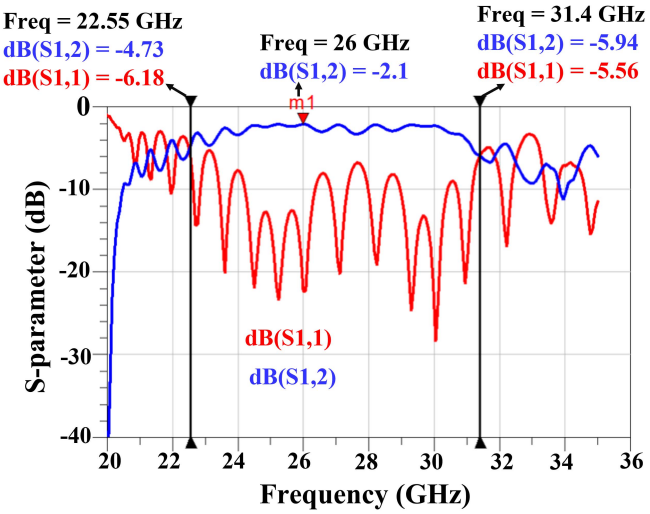

Fig. 22. Measurements of S_{12} (blue line) and S_{11} (red line) in the range 20–36 GHz for the layout shown in Fig. 21.

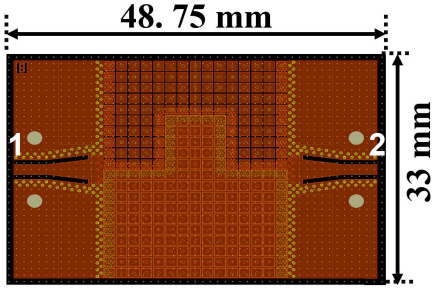

Fig. 23. Layout of the PTD-BEW path with 90° bends.

The layout in Fig. 21 is relevant to a longer PTD-BEW section, including 24 unit cells, for a total length of 63.6 mm. In this case, five mushroom unit cells are considered in the transverse direction. The relevant measured results can be seen in Fig. 22. The structure exhibits an insertion loss of around −2 dB, with a good matching between 24 and 26.5 GHz and between 29 and 30.8 GHz.

B. Segmented PTD-SEW Structure

The layout of a segmented PTD-BEW structure is presented in Fig. 23. The path is constituted by a single square meander, with four 90° bends. This layout is analogous to the one in the

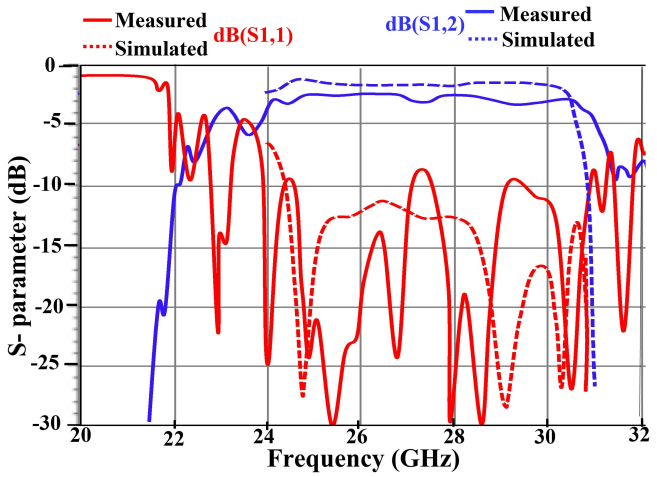

Fig. 24. Measurements of S_{12} (blue line) and S_{11} (red line) in the range 20–36 GHz.

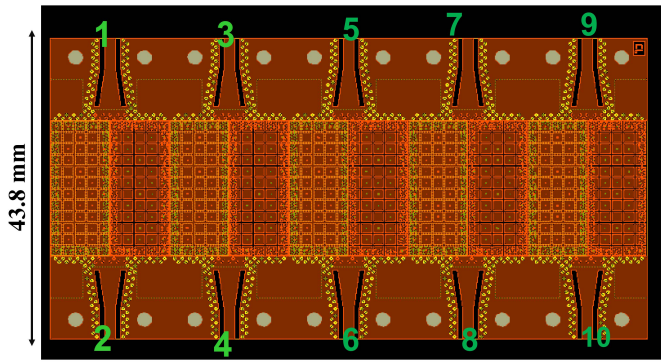

Fig. 25. Layout of the multiple PTD-BEW structure.

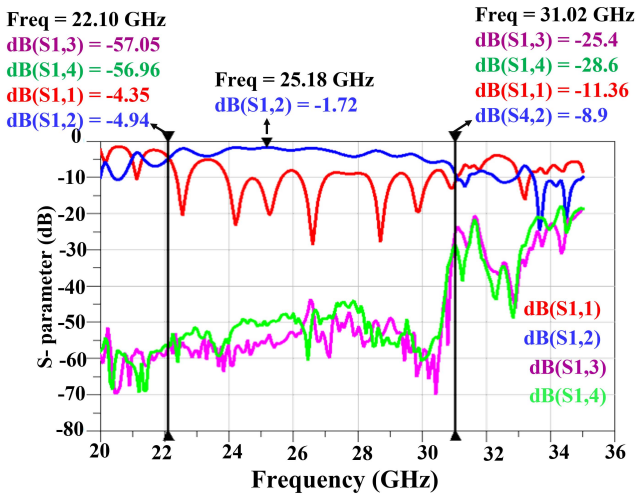

Fig. 26. Measurements of S_{12} (blue line), S_{11} (red line), S_{14} (green line), and S_{13} (magenta line) in the range 20–36 GHz.

example given in Fig. 8 and is used to test the robustness of the propagation against discontinuities in the path. Despite the abrupt discontinuities provided by the four right-angle bends, measurements in Fig. 24 show the same level of matching seen for the straight path (around −10 dB in the range from 24 to 31 GHz) with −2 dB of insertion loss.

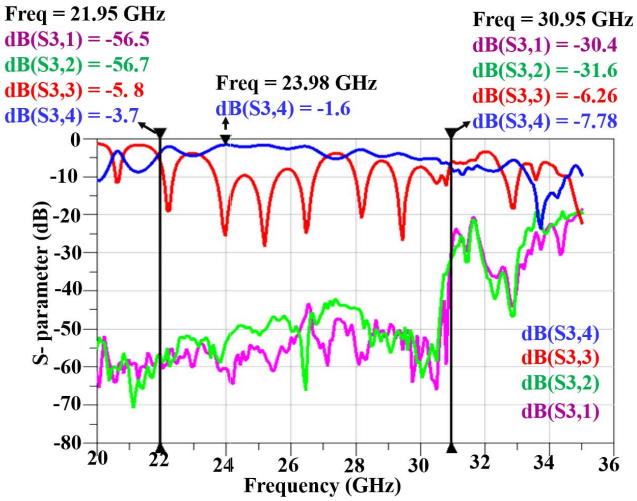

Fig. 27. Measurements of S_{34} (blue line), S_{33} (red line), S_{32} (green line), and S_{31} (magenta line) in the range 20–36 GHz.

C. Multiple PTD-BEW

The last structure analyzed consists of an arrangement of adjacent PTD-BEW sections and its layout is shown in Fig. 25. The distance between adjacent lines is about 16 mm, corresponding to about one wavelength at the lowest frequency of the bandwidth. It can be seen from Figs. 26 and 27 that the measured level of cross-coupling has an average value of −50 dB in the range 20–30 GHz, with a maximum value of −45 dB. The transmission coefficient is around −1.7 dB.

VI. Conclusion

The experimental verification of robust propagation in the PTD-symmetric BEW proposed in [11] has been carried out in this article. The practical feasibility of the structure has been demonstrated in the range between 22 and 32 GHz. For practical implementation, mushroom metasurfaces have been used to emulate the PMC BCs. The analyzed structures include a transmission line with bends and multiport junctions. Despite the passivity and the absence of nonreciprocal elements, the PTD-BEW is immune from reflections for those discontinuities which respect to the PTD symmetry. Thanks to this property, it is possible to guide the bifilar mode along bent paths with low insertion loss and good matching. In the simulations of the structures, we did not include any losses, because our focus was on the demonstration of the backscattering protection feature. In the fabricated structure, we had some losses that were caused by two sources: 1) finite conductivity of the metal and 2) losses in the dielectric. Leakage toward the lateral PPWs, on the other hand, is prevented due to the existence of a bandgap. It is also worth noting that other types of bandgap structures, such as the ones used in gap WG technology, could be used to reduce losses. This is currently being considered and will be the subject of future work. It should also be noted that the leakage in the lateral structures is prevented only in the bandgap region, which represents a limit to the operational bandwidth of any device that uses the PTD-BEW, such as beamformers or couplers. In spite of the many criticalities related to manufacturing, experimental

results have been found fully satisfactory. This paves the way for the possibility of designing new microwave devices with low return losses up to the Ka-band.

ACKNOWLEDGMENT

The activity has been carried out in the framework of the Joint Innovation Antenna Laboratory between Huawei Technologies, Milan, Italy, and the University of Siena, Siena, Italy.

REFERENCES

[1] F. D. M. Haldane, "Nobel lecture: Topological quantum matter," *Rev. Mod. Phys.*, vol. 89, no. 4, 2017, Art. no. 040502.
[2] Z. Wang, Y. Chong, J. D. Joannopoulos, and M. Soljačić, "Observation of unidirectional backscattering-immune topological electromagnetic states," *Nature*, vol. 461, no. 7265, pp. 772–775, Oct. 2009.
[3] H. Lira, Z. Yu, S. Fan, and M. Lipson, "Electrically driven nonreciprocity induced by interband photonic transition on a silicon chip," *Phys. Rev. Lett.*, vol. 109, no. 3, 2012, Art. no. 033901.
[4] M. C. Rechtsman *et al.*, "Photonic Floquet topological insulators," *Nature*, vol. 496, no. 7444, pp. 196–200, Apr. 2013.
[5] X. Cheng, C. Jouvaud, X. Ni, S. H. Mousavi, A. Z. Genack, and A. B. Khanikaev, "Robust reconfigurable electromagnetic pathways within a photonic topological insulator," *Nature Mater.*, vol. 15, no. 5, pp. 542–548, 2016.
[6] M. G. Silveirinha, "Z_2 topological index for continuous photonic materials," *Phys. Rev. B, Condens. Matter*, vol. 93, Feb. 2016, Art. no. 075110.
[7] A. B. Khanikaev, S. H. Mousavi, W.-K. Tse, M. Kargarian, A. H. MacDonald, and G. Shvets, "Photonic topological insulators," *Nature Mater.*, vol. 12, no. 3, pp. 233–239, 2013.
[8] M. G. Silveirinha, "$P.T.D$ symmetry-protected scattering anomaly in optic," *Phys. Rev. B, Condens. Matter*, vol. 95, Jan. 2017, Art. no. 035153.
[9] W.-J. Chen, Z.-Q. Zhang, J.-W. Dong, and C. T. Chan, "Symmetry-protected transport in a pseudospin-polarized waveguide," *Nature Commun.*, vol. 6, no. 1, pp. 1–8, Sep. 2015.
[10] D. J. Bisharat and D. F. Sievenpiper, "Guiding waves along an infinitesimal line between impedance surfaces," *Phys. Rev. Lett.*, vol. 119, no. 10, 2017, Art. no. 106802.
[11] E. Martini, M. G. Silveirinha, and S. Maci, "Exact solution for the protected TEM edge mode in a PTD-symmetric parallel-plate waveguide," *IEEE Trans. Antennas Propag.*, vol. 67, no. 2, pp. 1035–1044, Feb. 2019.
[12] Z. Xu *et al.*, "Line waves existing at junctions of dual-impedance metasurfaces," *ACS Photon.*, vol. 8, no. 8, pp. 2285–2293, Jun. 2021.
[13] I. Nadeem, V. Valentina, E. Martini, A. Toccafondi, and S. Maci, "Active impedance of PTD-symmetric checkerboard type open ended waveguide array," in *Proc. IEEE 15th Eur. Conf. Antenna Propag. (EuCap)*, Mar. 2021.
[14] I. Nadeem, V. Valentina, E. Martini, A. Toccafondi, and S. Maci, "PTD-symmetric square-waveguide array based on complementary boundary conditions," in *Proc. 15th Int. Congr. Artif. Mater. Novel Wave Phenomena-Metamater.*, Aug. 2021.
[15] E. Martini, M. Silveirinha, and S. Maci, "Transformation method for PTD symmetric edge waveguide," in *Proc. 13th Eur. Conf. Antennas Propag. (EuCAP)*, Mar./Apr. 2019, pp. 1–3.
[16] D. Sievenpiper, L. Zhang, R. F. J. Broas, N. G. Alexopolous, and E. Yablonovitch, "High-impedance electromagnetic surfaces with a forbidden frequency band," *IEEE Trans. Microw. Theory Techn.*, vol. 47, no. 11, pp. 2059–2074, Nov. 1999.
[17] M. N. M. Kehn, M. Nannetti, A. Cucini, S. Maci, and P. S. Kildal, "Analysis of dispersion in dipole-FSS loaded hard rectangular waveguide," *IEEE Trans. Antennas Propag.*, vol. 54, no. 8, pp. 2275–2282, Aug. 2006.
[18] X.-P. Chen and K. Wu, "Low-loss ultra-wideband transition between conductor-backed coplanar waveguide and substrate integrated waveguide," in *IEEE MTT-S Int. Microw. Symp. Dig.*, Jun. 2009, pp. 349–352.
[19] Z. Wang, S. Adhikari, D. Dousset, C.-W. Park, and K. Wu, "Substrate integrated waveguide (SIW) power amplifier using CBCPW-to-SIW transition for matching network," in *IEEE MTT-S Int. Microw. Symp. Dig.*, Jun. 2012, pp. 1–3.
[20] F. Taringou, J. Bornemann, and K. Wu, "Broadband coplanar-waveguide and microstrip low-noise amplifier hybrid integrations for K-band substrate integrated waveguide applications on low-permittivity substrate," *IET Microw., Antennas Propag.*, vol. 8, no. 2, pp. 99–103, Jan. 2014.
[21] M. Salehi and E. Mehrshahi, "A closed-form formula for dispersion characteristics of fundamental SIW mode," *IEEE Microw. Wireless Compon. Lett.*, vol. 21, no. 1, pp. 4–6, Jan. 2011.
[22] D. Deslandes and K. Wu, "Accurate modeling, wave mechanisms, and design considerations of a substrate integrated waveguide," *IEEE Trans. Microw. Theory Techn.*, vol. 54, no. 6, pp. 2516–2526, Jun. 2006.

Iram Nadeem (Student Member, IEEE) received the B.S. degree in electrical engineering majoring in power systems and the M.S. degree in telecommunication engineering majoring in optical fiber communication from the University of Engineering and Technology (UET) Taxila, Taxila, Pakistan, in 2010 and 2014, respectively, and the M.Eng. degree in information and communication engineering from Chosun University, Gwangju, South Korea, in 2018, on full-time scholarship from the Korean Government. She is currently pursuing the Ph.D. degree with the Electromagnetics Innovation Joint Laboratory, Huawei, Milan, Italy, and the University of Siena, Siena, Italy.

She was a Visiting Researcher with the University Carlos III of Madrid, Madrid, Spain, to investigate gap-wave technology with parity time-reversal duality (PTD) symmetry. She worked as a Researcher with the Department of Information and Communication Engineering, Chosun University, from 2018 to 2019. She is actively working on higher-order symmetry type: PTD symmetric structures. Her research project was ultra-wideband antenna design for location detection applications. Moreover, she also worked as a Lecturer and a Laboratory Engineer in different engineering institutes in Pakistan from 2011 to 2015. Her research interests include PTD symmetric structures, gap-wave technology, UWB, and MIMO antenna design.

Ms. Nadeem was a recipient of "TICRA-EurAAP Grants-2022" and "Dr. Mojgan Daneshmand Grant-2022" based on her academic profile.

Valentina Verri received the B.Sc. and M.S. degrees in telecommunication engineering and the Ph.D. degree from Politecnico di Milano, Milan, Italy, in 2010, 2013, and 2016, respectively.

In 2013, she did an internship in CommScope, Rome, Italy. From 2015 to 2016, she was a Visiting Research Student with Aalto University, Espoo, Finland. She is currently a Microwave Technical Engineer with Huawei Technologies, Milan. Her research interests include antenna design for mmWave and THz applications.

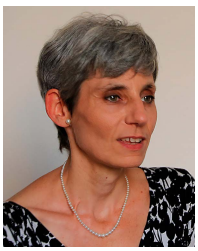

Enrica Martini (Senior Member, IEEE) was born in Spilimbergo, Pordenone, Italy, in 1973. She received the Laurea degree *(cum laude)* in telecommunication engineering from the University of Florence, Florence, Italy, in 1998, the Ph.D. degree in informatics and telecommunications from the University of Florence, and the Ph.D. degree in electronics from the University of Nice-Sophia Antipolis, Nice, France, in 2002, under joint supervision.

She worked under a one-year research grant with Alenia Aerospazio Company, Rome, Italy, until 1999. In 2002, she was appointed as a Research Associate with the University of Siena, Siena, Italy. In 2005, she received the Hans Christian Ørsted Post-Doctoral Fellowship from the Technical University of Denmark, Lyngby, Denmark. She joined the Electromagnetic Systems Section, Ørsted DTU Department, until 2007. From 2007 to 2017, she was a Post-Doctoral Fellow with the University of Siena. From 2016 to 2018, she was the CEO of the startup Wave Up S.r.l, Siena, which she co-founded in 2012. She is currently an Associate Professor with the University of Siena. Her research interests include metasurfaces, metamaterial characterization, electromagnetic scattering, antenna measurements, finite element methods, and tropospheric propagation.

Dr. Martini was a co-recipient of the 2016 Schelkunoff Transactions Prize Paper Award, the Best Paper Award in Antenna Design and Applications at the 11th European Conference on Antennas and Propagation in 2017, the Best Poster Award at the Metamaterials Congress in 2019, and the Best Paper Award in Electromagnetics at the 15th European Conference on Antennas and Propagation in 2021.

Fabio Morgia was born in Rome, Italy, in 1969. He received the Laurea degree in electronic engineering from the University of Rome, Rome, in 2000.

In 2001, he joined the Siemens Information and Communication Networks S.p.A, now Nokia Siemens Networks S.p.A., Cassina de' Pecchi, Milan, Italy, Research and Development Branch, with the function of "Microwave and RF Designer." Since March 2008, he has been with Huawei Technologies, Milan, where he now holds the position of an Antenna Designer for point-to-point radio links.

Alberto Toccafondi (Senior Member, IEEE) received the Laurea degree *(summa cum laude)* in electronic engineering and the Ph.D. degree in telecommunications and informatics from the University of Florence, Florence, Italy, in 1989, and 1994, respectively.

In 1995, he joined the Department of Information Engineering and Mathematics, University of Siena, Siena, Italy, where he is currently an Associate Professor. His research interests include antennas and microwave devices, and analytic and numerical techniques for electromagnetic scattering and multipath propagation prediction, especially incremental and asymptotic methods applied to the prediction of electromagnetic scattering, and the analysis and design of antennas and microwave devices.

Dr. Toccafondi served as a reviewer for many scientific journals. He is also an Associate Editor of the IEEE TRANSACTIONS ON ANTENNAS AND PROPAGATION. From 2002 to 2005, he served as a Secretary and a Treasurer for the Central and South Italy Section and the AP/Microwave Theory and Techniques (MTT) Joint Chapter of the IEEE. He served as a Treasurer from 2006 to 2007 and a Secretary from 2008 to 2009 for the established IEEE Italy Section.

Maurizio Mattivi was born in Castelnuovo del Garda, Verona, Italy, in April 1959. He received the M.Sc. degree in electronic engineering from the University of Bologna, Bologna, Italy, in 1985.

Since being graduated, he joined several first-tier companies, operating in the field of telecommunications: GTE (later SIEMENS), Munich, Germany till 1995, as an Optical Devices and Sub-Modules Designer; Italtel, Rome, Italy, till 1999, as an microwave (MW) Systems Engineer; and Siemens ICN (later Nokia), Espoo, Finland, till 2009. From 2009 to 2017, he has been the Head of MW and mmWave Team, Milan Research Center, Huawei, Milan, Italy. Since 2019, he has been the Director of MW and mmWave Competence Center, Huawei. He is the first author or a coauthor of more than 20 technical papers, and he also authored several presentations for workshops and International Conferences.

Stefano Maci (Fellow, IEEE) received the Laurea degree *(cum laude)* from the University of Florence, Florence, Italy, in 1987.

Since 1997, he has been a Professor with the University of Siena, Siena, Italy. Since 2000, he was a member of the Technical Advisory Board of 16 international conferences and the Review Board of six international journals. From 2004 to 2007, he was a work package (WP) Leader of the Antenna Center of Excellence (ACE, FP6-EU). From 2007 to 2010, he was an International Coordinator of a 24-Institution Consortium of a Marie Curie Action (FP6). In 2004, he was the Founder of the European School of Antennas (ESoA), a post-graduate school that presently comprises 34 courses on Antennas, Propagation, Electromagnetic Theory, and Computational Electromagnetics and 150 teachers coming from 15 countries. From 2008 to 2015, he was the Director of the Ph.D. Program in information engineering and mathematics with the University of Siena. From 2013 to 2015, he was a member of the first National Italian Committee for Qualification to Professor. Since 2004, he has been the Director of ESoA. His research activity is documented in 180 papers published in international journals (among which 100 in IEEE journals), ten book chapters, and about 450 papers in proceedings of international conferences. The papers he coauthored have been cited about 8800 times (H-index 48, source: Google Scholar). His research interests include high-frequency and beam representation methods, computational electromagnetics, large phased arrays, planar antennas, reflector antennas and feeds, metamaterials, and metasurfaces.

Prof. Maci has been a former member of the AdCom of IEEE Antennas and Propagation Society (AP-S) and the Antennas and Propagation Executive Board of the Institution of Engineering and Technology (IET), U.K., an Associate Editor of IEEE TRANSACTIONS ON ANTENNAS AND PROPAGATION, the Chair of the Award Committee of IEEE AP-S, and a member of the Board of Directors of the European Association on Antennas and Propagation (EurAAP). He founded and has been the Former Director of the consortium FORESEEN, involving 48 European Institutions. He was the Principal Investigator of the Future Emerging Technology Project "Nanoarchitectronics" of the eighth EU Framework program, and he is also a Principal Investigator of the EU program "Metamask." Since 2010, he has been a Principal Investigator of six cooperative projects and a University Coordinator of about other 20 cooperative projects financed by the European Space Agency. He was the Co-Founder of two spin-off companies. He has been a Distinguished Lecturer of the IEEE AP-S and a EuRAAP Distinguished Lecturer with the Ambassador Program. He was a recipient of the EurAAP Award in 2014, the IEEE Schelkunoff Transaction Prize in 2016, the Chen-To Tai Distinguished Educator Award in 2016, and the URSI Dellinger Gold Medal in 2020. He has been the TPC Chair of the METAMATERIAL 2020 Conference and a Designed Chairperson of EuCAP 2023. In the last ten years, he has been invited 25 times as a key-note speaker in international conferences. He is the President-Elect of the IEEE AP-S 2022.

Open Access funding provided by 'Università degli Studi di Siena' within the CRUI CARE Agreement